Journal of Magnetics 31(2), 195-203 (2026)

ISSN (Print) 1226-1750
ISSN (Online) 2233-6656
https://doi.org/10.4283/JMAG.2026.31.2.195

Improving Mesh Quality in Magnetic Force Calculation Using Element-Penetrating Virtual Air Gap Method

Gui Hwan Kim[1], Chang Hoon Seok[2], and Hong Soon Choi[3]*

[1]*Kyungpook National University, Department of Electrical Engineering, 80, Daehak-ro, Buk-gu, Daegu 41566, Republic of Korea*
[2]*Daegu Mechatronics & Materials Institute, 32, Seongseo Gongdan-ro 11-gil, Dalseo-gu, Daegu 42714, Republic of Korea*
[3]*Kyungpook National University, School of Electronic and Electrical Engineering, 80, Daehak-ro, Buk-gu, Daegu 41566, Republic of Korea*

(Received 5 November 2025, Received in final form 19 June 2026, Accepted 23 June 2026)

In the calculation of electric and magnetic forces using the finite element method (FEM), the number and quality—i.e., the shape—of elements are critical factors in the entire analysis process. However, element quality is inevitably constrained by the system's geometry. The finite element system includes not only the simulated object but also the region of interest (ROI) where magnetic forces are evaluated. If the elements are generated prior to defining the ROI, a mesh better suited for computation is obtained. We present a method for constructing a high-quality meshing environment for magnetic force problems based on this approach. In such cases, the boundary of the ROI for magnetic force may penetrate through the interior of elements. To ensure validity and accuracy, the concept of a virtual air gap (VAG), developed in previous studies, is required. We propose a method that incorporates the VAG concept and demonstrate its application and effectiveness through numerical examples using mesh quality measures.

Keywords : virtual air gap, region of interest, Maxwell stress tensor, finite element, magnetic force

1. Introduction

Electromagnetic force computation is a necessary aspect of the research and development of electrical devices, including generators and motors, sensors and actuators [1, 2], as well as magnetorheological and optical instruments [3–5]. It is essential for analyzing mechanical characteristics such as displacement, rotation, vibration, fatigue, and failure at both component and system levels. The calculation of electromagnetic force can be achieved through various approaches, including the Maxwell stress tensor (MST) method, the virtual work principle [6], the Kelvin force density formula [7], the equivalent magnetized source [8], and the equivalent magnetization current method [9]. All these approaches yield consistent electromagnetic force values when applied to the same object within the same system [9, 10]. Among them, the MST method is the most widely adopted in numerical analyses such as finite element simulations, due to its convenience in expressing the force as a surface integral.

Finite element analysis considers mesh quality as a crucial factor for computational feasibility, simulation efficiency, and the accuracy of the results. Mesh quality is typically assessed based on the number and shape of elements [10–12]. Achieving a high-quality mesh often requires tuning of meshing algorithms, simplifying model geometry, and heuristic techniques such as eliminating internal boundaries within homogeneous materials. We present an alternative approach; electromagnetic force calculations require the definition of a region of interest (ROI), which serves as the target domain. The ROI, however, often interferes with the generation of a high-quality mesh in conventional simulation workflows. Rather than defining the ROI prior to mesh generation—as is customary in the pre-processing stage—the proposed approach specifies the ROI after meshing, as part of the post-processing stage. In this configuration, the ROI boundary may intersect internal elements, but the high fidelity of field values within well-shaped elements ensures accurate electromagnetic force calculations.

Incorporating the concept of a virtual air gap (VAG) [13] enables flexible selection of the ROI even within

*Corresponding author: Tel: +82-53-950-7231
e-mail: tochs@knu.ac.kr

magnetic materials, thereby allowing mesh quality improvements to be achieved under a broader range of conditions. This approach also addresses issues that arise when the ROI is in contact with, embedded within, or located inside magnetic materials [14]. Accordingly, the proposed methodology incorporates the concept of the VAG.

Section II of this paper examines the characteristics of the MST method, selected among various electromagnetic force computation techniques. Mesh quality considerations are then summarized, followed by a discussion of the VAG. In Section III, the proposed framework is introduced in which the ROI is determined during the post-processing stage, hereafter referred to as the *post-processing approach.* This idea is validated through two numerical analyses in Section IV, demonstrating its effectiveness in maintaining computational accuracy and achieving high-quality mesh generation. For simplicity, the discussion is confined to magnetostatic systems. The presented methodology, however, is applicable to other force computation techniques. Moreover, since the mathematical structure is identical, it can also be extended to the case of electrostatic and optical electromagnetic force analyses.

2. Maxwell Stress Tensor Method: Limitations and Resolution via Virtual Air Gap Concept

2.1. Overview of the Maxwell Stress Tensor Method

As mentioned in the introduction, various methods exist for computing the electromagnetic force acting on objects, among which the MST method is most widely preferred. The MST is derived by transforming the Lorentz force equation into a surface integral and can be expressed as follows: The total magnetic force vector $\mathbf{F}_{\mathrm{m}}$ exerted on objects within a specific ROI Ω is evaluated using the following formula:

$$\mathbf{F}_{\mathrm{m}} = \oint_{\partial\Omega} \hat{\mathbf{n}} \cdot \overleftrightarrow{\mathbf{T}}_{\mathrm{M}} dS \tag{1}$$

Here, $\hat{\mathbf{n}}$ denotes the outward unit normal vector on the boundary $\partial\Omega$ of the ROI Ω and $\overleftrightarrow{\mathbf{T}}_{\mathrm{M}}$ represents the dyadic form of the MST, which is given by the following expression:

$$\overleftrightarrow{\mathbf{T}}_{\mathrm{M}} = \frac{1}{\mu_0}\left[\mathbf{B}\otimes\mathbf{B} - \frac{1}{2}(\mathbf{B}\cdot\mathbf{B})\overleftrightarrow{\mathbf{I}}\right], \tag{2}$$

where μ_0 is the permeability of free space, $\mathbf{B}$ is the magnetic flux density (or B-field), $\mathbf{B}\otimes\mathbf{B}$ and $\mathbf{B}\cdot\mathbf{B}$ are the dyadic product and dot product, respectively, and $\overline{\mathbf{I}}$ is the identity tensor. The characteristics of the MST method, as expressed in equation (1) and (2), are as follows:

- Various forms of the MST exist. Eq. (2) corresponds to the Lorentz form, while other well-known variants include the Einstein–Laub, Abraham–Minkowski, and Chu forms [15–18]. Although our analysis focuses on the Lorentz formulation, the proposed method can be generally applied to other tensor forms as well, owing to the characteristics of the VAG concept discussed later.
- In some references [15-18], a negative sign is introduced in the right-hand side of eq. (1), indicating a difference in convention regarding the treatment of electromagnetic momentum flow. In that case, the sign in eq. (2) is also adjusted to ensure consistency.
- Eqs. (1) and (2) are valid and guarantee accuracy in static systems. In dynamic systems, they are extended as follows:

$$\mathbf{F}_{\mathrm{m}} = \oint_{\partial\Omega} \hat{\mathbf{n}} \cdot \overleftrightarrow{\mathbf{T}}_{\mathrm{EM}} dS + \frac{d}{dt}\int_{\Omega} \mathbf{P}_{\mathrm{EM}} dV \tag{3}$$

where $\overleftrightarrow{\mathbf{T}}_{\mathrm{EM}}$ denotes the extended MST that includes electric field components, and $\mathbf{P}_{\mathrm{EM}}$ represents the electromagnetic momentum vector. The formalism of $\mathbf{P}_{\mathrm{EM}}$ within materials, in connection with $\overleftrightarrow{\mathbf{T}}_{\mathrm{EM}}$, remains the subject of unresolved controversies [15-18]. As this falls outside the scope of our discussion, we limit our analysis to static systems for the sake of simplicity.

The preference for the MST method originates from two main advantages: the use of a closed surface integral, which is more tractable than volume-based methods, and the absence of differential operators, which ensures numerical stability.

2.2. Element Quality in Finite Element Systems

In finite element systems, mesh quality serves as a criterion for evaluating numerical performance. One of the measurable factors is the number of elements, which should be sufficient to ensure accurate computation; however, an excessive number can negatively impact computational cost. Another crucial factor is the shape of the elements. In two-dimensional domains with triangular elements, the equilateral configuration is generally regarded as an ideal element. Unacceptably distorted shapes are termed *degenerated* [10–12]. Several numerical measures for evaluating such cases are provided; we adopt skewness, the surface versus circumradius (or the volume versus circumradius), and a condition number for each element. These quantities are scale-independent and normalized. The skewness, denoted by m_{skew}, is given as follows:

$$m_{\text{skew}} = 1 - \max\left(\frac{\theta_e - \Phi_e}{180^\circ - \Phi_e}, \frac{\Phi_e - \theta_e}{\Phi_e}\right), \tag{4}$$

where θ_e is the plane angle (2D) or dihedral angle (3D) of the element, and Φ_e corresponds to that of the ideal element. In two dimensions, for triangular, $\Phi_e = 60^\circ$. The surface versus circumradius (or volume versus circumradius), one of the aspect ratios, is given as follows:

$$m_{\text{SvC}} = \alpha_D \frac{(A_e)^{\frac{1}{D}}}{R_e}, \tag{5}$$

where α_D is a normalization factor with respect to the dimension number D, A_e is the area or volume of the element, and R_e is the circumradius of the element. For a two-dimensional triangular element, $\alpha_{D=2} = \sqrt{\frac{4}{3\sqrt{3}}}$. The condition number is given as follows [10, 12]:

$$m_{\text{cond}} = \frac{D|B_e|^{\frac{2}{D}}}{\| B_e \|_{\text{F}}^2}, \tag{6}$$

where B_e is the transformation matrix from the ideal element to the current element. $| B_e |$ and $\| B_e \|_{\text{F}}$ denote the determinant and the Frobenius norm of B_e, respectively.

Although high-quality mesh generation algorithms that account for these factors do exist, they are constrained by the domain defined within the system, either the physical region of the actual object or a user-defined virtual area, such as the ROI. As shown in Fig. 1, two notable issues

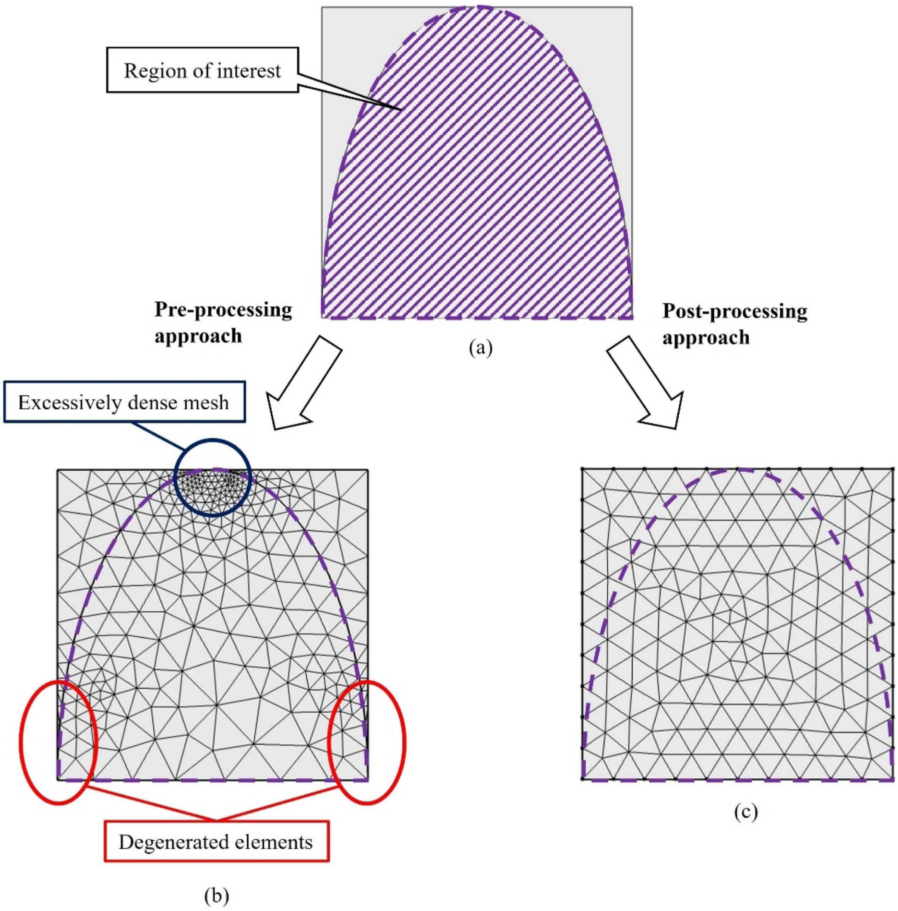

Fig. 1. (Color online) The boundary of the ROI within the magnetic material (purple dashed line) and the variation in element distribution depending on its generation sequence. Derived from (a), (b) illustrates the mesh generated after defining the boundary of the ROI, i.e., during the pre-processing stage. Particularly in confined regions, two types of abnormal elements—excessively dense and degenerated—are observed. (c) introduces the post-processing approach, a stage in which the mesh is generated prior to defining the boundary of the ROI. Compared to (b), a relatively well-formed meshing environment is achieved. Under this condition, the boundary of the ROI penetrates through the interior of the elements.

arise within designated regions where the boundaries come close together. One issue is excessive element density, which demands more computational resources without meaningful improvement in validity. Another is the occurrence of degenerated elements, making it difficult to obtain accurate and stable quantities. Typical work-arounds to these issues include either simplifying problematic boundaries or modifying mesh generation rules to mitigate element quality degradation. For example, sharp boundaries may be rounded, or the number of elements in specific regions may be explicitly assigned. Each approach has its limitations: the former may oversimplify physically sensitive areas, while the latter often faces a trade-off between element quantity and quality.

The method proposed in this paper is to form the ROI *after* mesh generation, as illustrated in Fig. 1(c). This allows the meshing algorithm to operate more flexibly, unconstrained by the boundaries of the ROI, while still preserving the physical interfaces. Though conceptually tied to conventional geometry simplification, the procedure delivers integrity-preserving results, since the physical quantities inside the meshes remain reliable under improved conditions.

2.3. VAG Concept for Force Evaluation Within Magnetic Materials

The MST method remains controversial in magnetic media, particularly when the ROI is located inside a material or in contact with another, as illustrated in Fig. 1. In such a case, one encounters the problem of determining which electromagnetic force calculation method is appropriate within the medium. Several versions of the MST, including Eq. (2), have been proposed for use within material interiors, yet none is commonly accepted as the definitive model for accurately describing electromagnetic forces in matter [15–18]. To address this unresolved problem, we introduce the concept of the VAG.

The VAG is defined as an infinitesimally thin, hypothetical surface composed of non-magnetic material. Fig. 2 presents the VAG and explains its conceptual application. It is applied to the boundary of the ROI created for the purpose of calculating electromagnetic force, corresponding to the integration surface in Eq. (1). Applying the VAG effectively encloses the interior of the ROI with a thin, hypothetical gap, thereby transforming the boundary of the ROI into a (hypothetical) cavity layer within the material. This transformation enables the MST method to operate under conditions that allow for the valid computation of magnetic force. Since the VAG is infinitesimally thin, it does not affect the surrounding space either inside or outside the gap.

The concept of the VAG centers on the magnetic fields within the gap, denoted as $\mathbf{B}_v$ and $\mathbf{H}_v$, respectively. These fields can be determined by applying magnetic boundary conditions between the VAG and the adjacent inner surface. (An identical form of the equations is also derived from the boundary conditions with the outer region.) Thus,

$$\mathbf{B}_v = (\mathbf{B}\cdot\hat{\mathbf{n}})\hat{\mathbf{n}} + \mu_0(\mathbf{H}\cdot\hat{\mathbf{t}})\hat{\mathbf{t}} + \mu_0(\mathbf{H}\cdot\hat{\mathbf{u}})\hat{\mathbf{u}}, \tag{7}$$

$$\mathbf{H}_v = \frac{1}{\mu_0}(\mathbf{B}\cdot\hat{\mathbf{n}})\hat{\mathbf{n}} + (\mathbf{H}\cdot\hat{\mathbf{t}})\hat{\mathbf{t}} + (\mathbf{H}\cdot\hat{\mathbf{u}})\hat{\mathbf{u}}, \tag{8}$$

where $\hat{\mathbf{n}}$ is the normal vector to the surface of the VAG, and $\hat{\mathbf{t}}$ and $\hat{\mathbf{u}}$ are two mutually orthogonal tangential vectors. In this hypothetical nonmagnetic layer, the relation $\mathbf{B}_v=\mu_0\mathbf{H}_v$ holds. Furthermore, when the VAG is formed in *actual* nonmagnetic domain, the fields revert to $\mathbf{B}_v=\mathbf{B}$ and $\mathbf{H}_v=\mathbf{H}$.

All electromagnetic force calculation methods can be applied to the VAG. Despite differences in their formulations, they consistently yield the same valid magnetic force value [13, 19–21]. Among these, the MST method operates on the principle that the entire integration surface in Eq. (1) is replaced by the VAG. In this case, the MST $\overleftrightarrow{\mathbf{T}}_{\mathrm{M}}$ within the VAG is modified in Eq. (2) as follows:

$$\overleftrightarrow{\mathbf{T}}_{\mathrm{M,v}} = \frac{1}{\mu_0}\left[\mathbf{B}_v \otimes \mathbf{B}_v - \frac{1}{2}(\mathbf{B}_v\cdot\mathbf{B}_v)\overleftrightarrow{\mathbf{I}}\right]. \tag{9}$$

The integrand in Eq. (1) is effectively replaced by $\overleftrightarrow{\mathbf{T}}_{\mathrm{M,v}}$ as defined in Eq. (9). In vacuum, $\overleftrightarrow{\mathbf{T}}_{\mathrm{M,v}}$ reverts to the original tensor $\overleftrightarrow{\mathbf{T}}_{\mathrm{M}}$. Other formulations of the MST, beyond the Lorentz form, also conform to the Eq. (9), provided that the material properties are substituted with those of vacuum when applying the VAG concept. This aligns with the fact that any form of the MST yields the same accurate magnetic force when applied to an isolated object in vacuum. Furthermore, $\overleftrightarrow{\mathbf{T}}_{\mathrm{M,v}}=\overleftrightarrow{\mathbf{T}}_{\mathrm{M}}$ in nonmagnetic media, indicating that the VAG concept retains its generality even outside material boundaries.

We further validate $\overleftrightarrow{\mathbf{T}}_{\mathrm{M,v}}$ against $\overleftrightarrow{\mathbf{T}}_{\mathrm{M}}$ in Section IV.1, continuing previous studies in [13, 19-21].

3. Proposed Concept

The proposed concept is as follows: while the steps for model construction and material property definition remain unchanged in finite element modeling, the specification of the ROI for magnetic force is deferred until *after* mesh generation (and after solving the governing

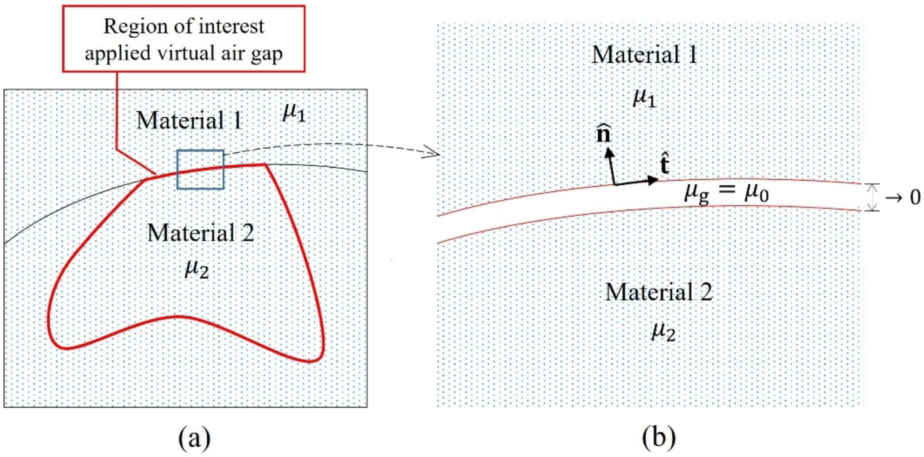

Fig. 2. (Color online) A diagram of the VAG concept. (a) The red line represents the boundary of the ROI for magnetic force calculation, corresponding to the integration surface in Eq. (1). When the VAG concept is applied, the gap is generated along this red line, resulting in the ROI being isolated by the void area. (b) is a magnified view of the boxed area in (a), shown at a microscopic scale. Within the VAG whose thickness approaches zero, two types of magnetic fields are described by Eqs. (7) and (8), respectively. Accordingly, the MST in Eq. (2) takes the form of Eq. (9).

equation). That is, as illustrated in Fig. 1(c), the boundary of the ROI is formed to pass through the interior of the elements. In this paper, we refer to this approach as ROI modeling in post-processing stage, or simply, the *post-processing approach*. The conventional approach shown in Fig. 1(b) is, conversely, referred to as the *pre-processing approach*.

When Eq. (1) is applied to the ROI, the VAG concept is

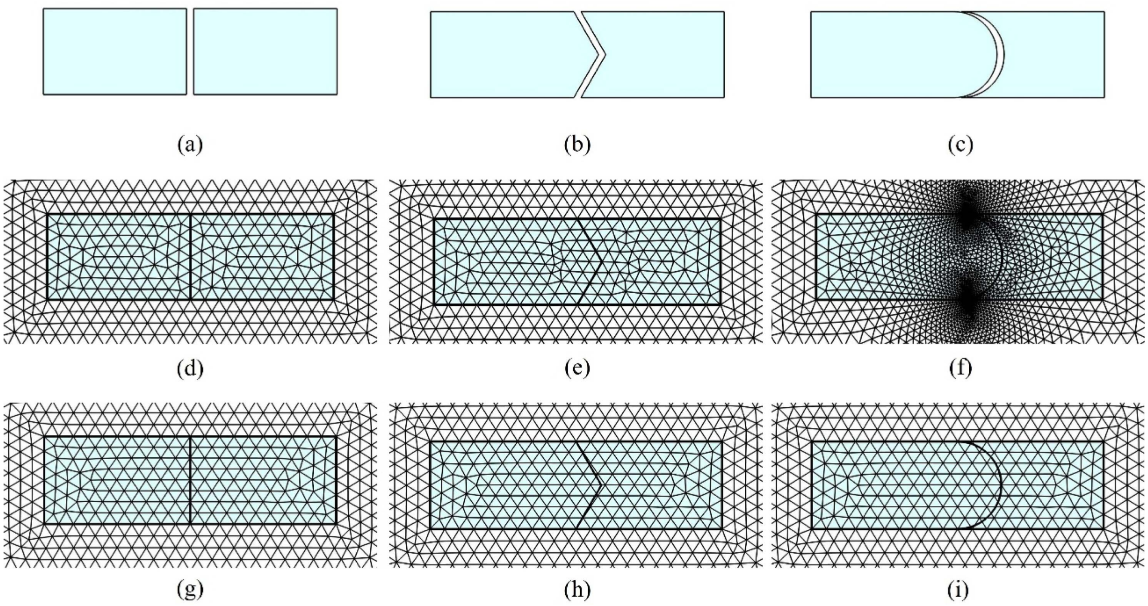

Fig. 3. (Color online) Validation Model 1. (a), (b), and (c): Two-dimensional validation models. In all cases, two objects are positioned facing each other at a distance *d*. Both simulate ferrite magnets characterized by a relative permeability of 1.05 and a remanent flux density of 0.3 T, directed horizontally to the right. The external air region is a 100 cm square. In this model, the magnetic force per unit centimeter is evaluated relative to the left object. The contact surface shapes are as follows: (a) a planar surface, (b) a wedge with a base length of 3 cm and a height of 3 × tan(π/6) cm, and (c) a semicircular shape with a radius of 3 cm. (d), (e), and (f): Element generation results for each contact model. In particular, (f) shows excessive element generation along the edge of the contact surface. (g), (h), and (i): Results for each contact model obtained by assigning the boundary of the ROI after mesh generation. In these cases, the contact boundary intersects the generated elements. For the remaining non-contact cases ($d > 0$), conventional meshing is performed.

integrated with the post-processing approach, as the computation covers vacuum as well as magnetic media. The MST in Eq. (9) is formally associated with the ROI. Thus, the magnetic fields from Eqs. (7) and (8), evaluated at a given point, are specified with respect to the normal and tangential vectors of the ROI shaped there.

One advantage of the post-processing approach is that it avoids the generation of low-quality elements caused by the ROI. In addition, modifications to the ROI do not necessitate remeshing or re-solving. Reliable magnetic force results are still ensured, even with this flexibility, as Eq. (9) contains no differential operators. This allows tensor values to remain accurate even when evaluated directly from the field within each element.

4. Numerical Analysis

In this section, we demonstrate the suitability of the post-processing approach, along with the validation of $\overleftrightarrow{\mathbf{T}}_{M,v}$. Here, we compare performance using the mesh quality measures provided in Eqs. (4)-(6). Elements are generated through the advancing front algorithm. The simulations were performed using COMSOL Multiphysics.

4.1. Validation Model 1

The first validation model in Fig. 3 consists of two separate ferrite magnets, each having a contact surface with one of three different shapes. Both magnets are assumed to be uniformly magnetized in the rightward horizontal direction with a magnitude of 0.3 T. In this example, we calculated the magnetic force acting on the left object (per centimeter) for each contact surface as a function of the separation distance *d*. At the contact ($d = 0$), three different calculation procedures are implemented. The first uses the conventional MST $\overleftrightarrow{\mathbf{T}}_{M}$ described in Eq. (2). The second employs the MST with the VAG concept $\overleftrightarrow{\mathbf{T}}_{M,v}$ defined in Eq. (9), where the ROI is treated in the pre-processing stage, resulting in the elements being arranged along the contact surface, as illustrated in Fig. 3(d), (e), and (f). The third also uses Eq. (9), but the ROI is handled in the post-processing stage, resulting in the elements being placed before the contact surface, as illustrated in Fig. 3(g), (h), and (i). In this case, the contact surface passes through the interior of the elements. The purpose of comparing these three procedures is to reaffirm $\overleftrightarrow{\mathbf{T}}_{M,v}$ with respect to $\overleftrightarrow{\mathbf{T}}_{M}$, and to demonstrate that the approach illustrated in Fig. 3(g), (h), and (i) preserves such validity. Magnetic force graphs are presented in Fig. 4. The magnetic contact forces obtained through the pre- and post-processing approaches at the contact are summarized in Table 1, and the mesh quantities and quality measures are in Table 2.

Figure 4 presents the magnetic force acting on one of the two objects (specifically, the left one) as a function of distance *d*, categorized by the contact surface's shape.

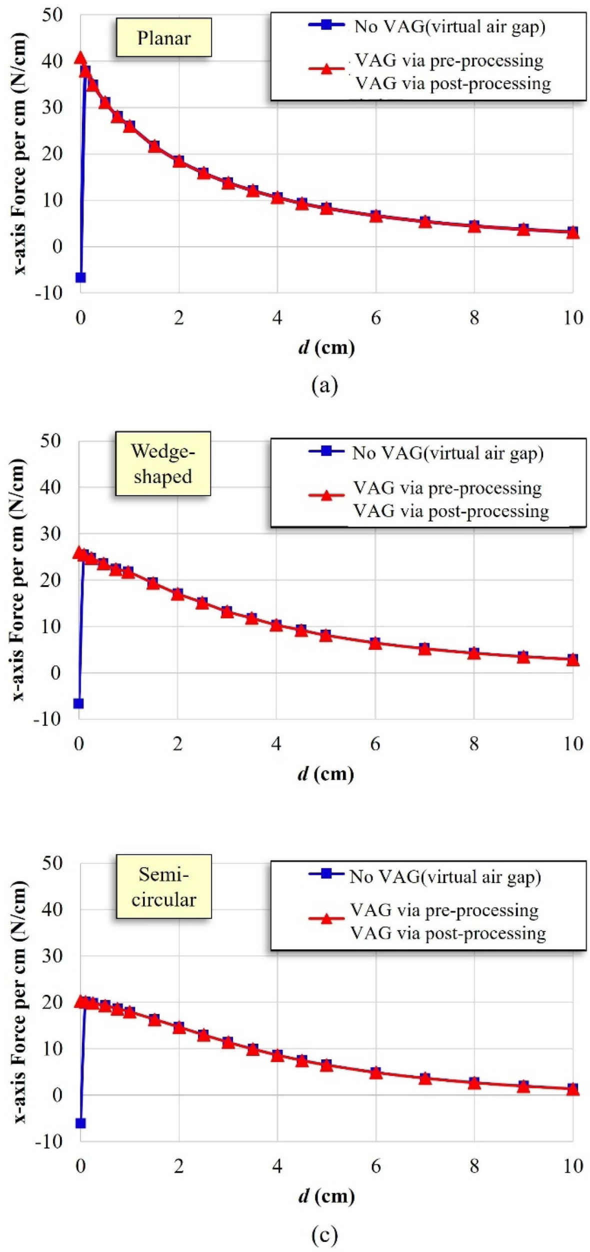

Fig. 4. (Color online) Magnetic force per unit centimeter calculated in Fig. 3 for three contact geometries: (a) planar, (b) wedge-shaped, and (c) semicircular. Each graph presents the magnetic force computed via the MST, comparing results without (blue line) and with the VAG (red line). Since the results obtained through both the pre- and post-processing approaches are identical when the VAG is applied, they are plotted together (see Table 1). In all cases, the application of the VAG produces a continuous trend in the magnetic force. Without it, the forces change discontinuously at the contact.

Table 1. Following Fig. 4, this table presents the magnetic force per unit centimeter for Validation Model 1 at contact ($d = 0$), shown in Fig. 3. The quantities are computed using the MST under three distinct setups: the cases without VAG and with VAG via the pre-processing approach (Figs. 3(d)–(f)); and with VAG via the post-processing approach (Figs. 3(g)–(i)). For each contact geometry, the pre- and post-processing approaches yield identical contact magnetic force values. This confirms that the post-processing approach can also produce accurate results. In particular, for the semicircular contact surface, it significantly improves the quality of the elements.

	No VAG	VAG via pre-processing	VAG via post-processing
Planar	-6.708	40.853	40.858
Wedgeshape	-6.623	26.044	26.038
Semicircle	-6.140	20.255	20.420

*Unit: N/cm

Each graph includes two sets of results depending on whether the VAG is applied. It can be observed that when the VAG is applied (i.e., when using $\overleftrightarrow{\mathbf{T}}_{\mathrm{M,v}}$), the magnetic force values at contact follow a trend consistent with the pre-contact behavior. This reflects the fact that the magnetic force varies continuously with distance. In contrast, the results obtained without the VAG, using $\overleftrightarrow{\mathbf{T}}_{\mathrm{M}}$, exhibit discontinuous changes across the contact point for all geometries. Moreover, the contact force remains unchanged regardless of the contact surface's shape. Fig. 4 reaffirms the validity of the VAG concept, aligning with previous studies. To elaborate, not only Eq. (2) but also other forms of MSTs without the VAG—such as the Einstein-Laub, Abraham-Minkowski, and Chu formulations—exhibit discontinuities across the contact point, similar to Eq. (2). This behavior stems from the absence of tangential and normal vector components in their tensor expressions, which distinguishes them from Eq. (9). As with Eq. (2), applying the VAG concept to these formulations resolves the discontinuity issue.

For the contact case, the invalidity of the conventional No-VAG approach is associated with the debate on the MST in materials, which is discussed in reference [23].

Table 1 lists the magnetic force (per centimeter) at contact ($d = 0$) extracted from Fig. 4. The magnetic force is calculated for each contact surface using three different procedures. The first data column represents the results from $\overleftrightarrow{\mathbf{T}}_{\mathrm{M}}$, which correspond to the $d = 0$ point on the blue curve in Fig. 4. As previously discussed, their values are not physically valid. The second data column shows the contact magnetic force calculated using $\overleftrightarrow{\mathbf{T}}_{\mathrm{M,v}}$, where the ROI is defined before the mesh generation, that is, using the pre-processing approach. The last column presents the contact magnetic force also based on $\overleftrightarrow{\mathbf{T}}_{\mathrm{M,v}}$, but with the ROI defined after the mesh generation, corresponding to the post-processing approach. Both approaches yield magnetic force values with less than 1 % deviation across different contact surfaces. Notably, as seen in Table 2, the semicircular shape allows for markedly better mesh quality measures while still yielding consistent magnetic force results.

4.2. Validation Model 2

Figure 5 shows a 4-pole, 12-slot interior permanent magnet motor. The stator and rotor cores are made of 35PN440 steel, and the permanent magnets are modeled as ferrite with a remanent flux density of 1.05 T. The motor height is set to 5 cm. In this model, the partial

Table 2. Number of elements and quality measures defined in Eqs. (4)-(6) for Validation Model 1 at contact ($d = 0$), shown in Fig. 3. Here, element counts are classified as the total and those in the two objects. The pre-processing approach related values correspond to Fig. 3(d)-(f), whereas the postprocessing ones correspond to Fig. 3(g)-(i). The three contact shapes under the postprocessing employ an identical mesh. Pronounced improvement of each quantity in the semicircular region demonstrates that the postprocessing provides a notable efficiency and quality improvement through the removal of degenerated elements.

	Total elements	Elements in two objects		m_{skew}	m_{SvC}	m_{cond}
Planar*	26,266	320	Minimum	0.657	0.754	0.857
			Average	0.949	0.990	0.994
Wedgeshape*	26,282	336	Minimum	0.657	0.754	0.857
			Average	0.949	0.990	0.994
Semicircle*	29,880	1,818	Minimum	0.024	0.017	0.044
			Average	0.940	0.988	0.992
Postprocessing	26,266	320	Minimum	0.657	0.754	0.857
			Average	0.946	0.990	0.994

*Evaluated using the pre-processing approach.

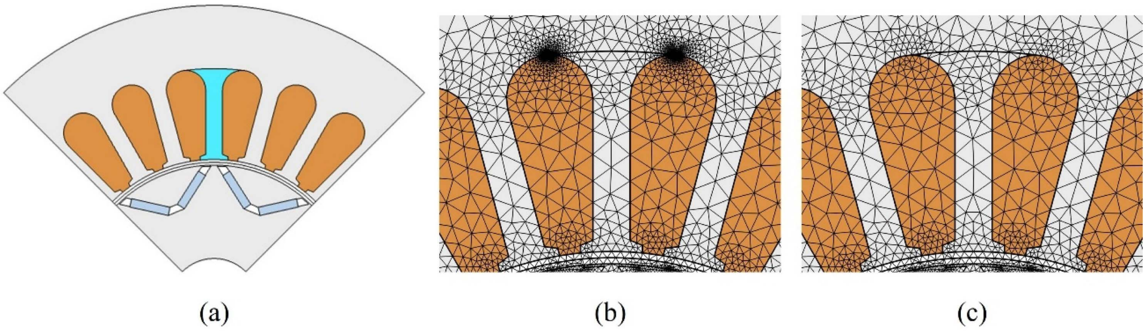

Fig. 5. (Color online) Validation Model 2. (a) One-quarter scale model of a 4-pole, 12-slot interior permanent magnet synchronous motor (IPMSM) used in verification model 2. The stator core is made of 35PN440 steel, and the permanent magnets are modeled with a remanent flux density of 1.05 T. The overall height of the model is 5 cm. In this model, the magnetic torque of the center tooth, highlighted in light blue, is calculated over a rotor mechanical angle range of 0-90 degrees. (b) Mesh distribution used in the pre-processing approach. (c) Mesh distribution used in the post-processing approach. The VAG is applied to the boundary marked between the teeth and the body.

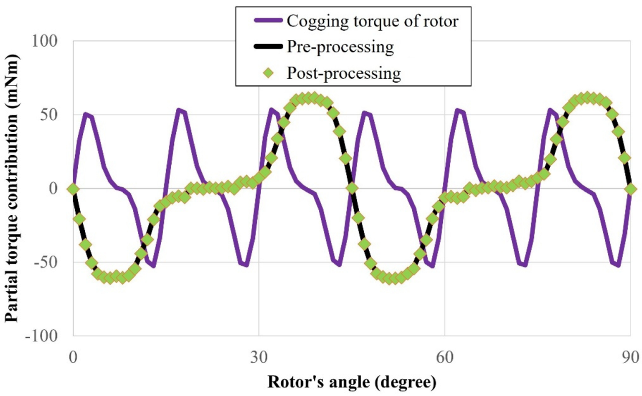

Fig. 6. Partial torque contribution of the designated tooth under no-current conditions, as calculated in Fig. 5, with the cogging torque for scale comparison. This graph shows that the post-processing approach achieves identical torque values to the pre-processing method, while significantly reducing the element count and improving mesh conditions.

magnetic torque contribution acting on a single tooth specified in Fig. 5(a) was calculated without current. This approach refers to previous studies on magnetic forces that induce tooth vibration [24–26]. The magnetic torques are presented in Fig. 6, and mesh quality measures are reported in Table 3. Fig. 6, which includes the cogging torque of the rotor for scale comparison, indicates that both the pre- and the post-processing approaches yield identical torque contribution values. In this case, the total number of elements for the two methods are 226,404 and 28,198, respectively, meaning that the post-processing approach reduces the element count to one-eighth of the original mesh. Degenerated elements are absent, as evidenced by the element quality measures in Table 3. Compared to Validation Model 1, the reduction is more significant because the overall domain in Fig. 5 is much smaller than that in Fig. 3.

5. Conclusion

In finite element analysis of magnetic force, predefining the ROI can hinder the generation of high-quality mesh elements and negatively affect computational accuracy. This study demonstrated that, by employing the VAG concept, accurate magnetic force computation is also achievable by setting the ROI after mesh generation through the post-processing procedure. The VAG concept

Table 3. From Validation Model 2, Number of elements and quality measures defined in Eqs. (4)-(6) are denoted under the conditions shown in Fig. 5. The pre- and post-processing approaches correspond to Figs. 5(b) and 5(c), respectively. The mesh remains fixed during the rotor angular displacement. In this test, the post-processing approach establishes significantly more favorable conditions than in the earlier setup.

	Total elements		m_{skew}	m_{SvC}	m_{cond}
Pre-processing approach	226,404	Minimum	1.386×10^{-4}	1.808×10^{-6}	2.151×10^{-4}
		Average	0.825	0.929	0.951
Post-processing approach	28,198	Minimum	0.518	0.617	0.772
		Average	0.879	0.966	0.977

serves as a remedy for unresolved issues that arise when the ROI boundary lies within magnetic materials. Two examples presented in this paper demonstrate that the post-processing approach can improve element quality in situations where low-quality mesh elements are observed. The methodology proposed in this study is expected to enable magnetic force analysis for components and parts in electrical machines that are otherwise difficult to compute. Furthermore, the same principle can be applied to electrostatic force calculations in static electric fields with similar equation structures, as well as to force evaluation in optics using the electromagnetic stress tensor.

References

[1] J. R. Melcher, Continuum Electromechanics. Vol. 2. Cambridge, MA: MIT press (1981) pp. 2.1~2.54.
[2] J. R. Brauer, Magnetic actuators and sensors. John Wiley and Sons, (2006) pp. 51~68.
[3] C.-W. Qiu, W. Ding, M. R. C. Mahdy, D. Gao, T. Zhang, F. C. Cheong, A. Dogariu, Z. Wang, and C. T. Lim, Light: Science and Applications **4**, e278 (2015).
[4] P. Polimeno, A. Magazzù, M. A. Iatì, F. Patti, R. Saija, C. D. Esposti Boschi, M. G. Donato, P. G. Gucciardi, P. H. Jones, G. Volpe, and O. M. Maragò, J. Quant. Spectrosc. Radiat. Transf. **218**, 131 (2018).
[5] D. E. Fernandes and G. S. Mario, Phys. Rev. A **91**, 061801 (2015).
[6] J. Coulomb, IEEE Trans. Magn. **19**, 2514 (1983).
[7] M. Liu, Phys. Rev. Lett. **84**, 2762 (2000).
[8] T. H. Boyer, Am. J. Phys. **56**, 688 (1988).
[9] T. Kabashina, A. Kawahara, and T. Goto, IEEE Trans. Magn. **24**, 451 (1988).
[10] P. M. Knupp, 45th AIAA Aerospace Sciences Meeting and Exhibit **SAND2007-8128C**, 1 (2007).
[11] J. R. Shewchuk, 11th International Meshing Roundtable, 115 (2002).
[12] A. Johnen, C. Geuzaine, T. Toulorge, and J. F. Remacle, Computer-Aided Design **103**, 24 (2018).
[13] H. S. Choi, I. H. Park, and S. H. Lee, IEEE Trans. Magn. **42**, 663 (2006).
[14] W. F. Brown, Magnetoelastic interactions. Springer, Berlin (1966) pp. 8~27.
[15] M. Bethune-Waddell and K. J. Chau, Reports on Progress in Physics **78**, 122401 (2015).
[16] M. Mansuripur, Applied Physics A **123**, 653 (2017).
[17] M. R. C. Mahdy, D. Gao, W. Ding, M. Q. Mehmood, M. Nieto-Vesperinas, and C.-W. Qiu, (2015). arXiv:1509.06971.
[18] B. A. Kemp and C. J. Sheppard, Advanced Electromagnetics **6**, 11 (2017).
[19] H. S. Choi, I. H. Park, and S. H. Lee, IEEE Transactions on Applied Super-conductivity **16**, 1832 (2006).
[20] H. S. Choi, S. H. Lee, Y. S. Kim, K. T. Kim, and I. H. Park, IEEE Trans. Magn. **44**, 1286 (2008).
[21] B. S. Park, H. S. Choi, J. O. Park, J. H. Wang, and I. H. Park, IEEE Trans. Magn. **56**, 1 (2020).
[22] J. H. Seo and H. S. Choi, IEEE Trans. Magn. **50**, 525 (2014).
[23] C. Rinaldi and H. Brenner, Phys. Rev. E **65**, 036615 (2002).
[24] Y. Chen, Y. Yang, and Y. Shen, Energies **11**, 2462 (2018).
[25] J. Hong, S. Wang, Y. Sun, and H. Cao, IEEE Trans. Ind. Appl. **57**, 3678 (2021).
[26] H. S. Choi, J. H. Lee, and I. H. Park, IEEE Trans. Magn. **41**, 1464 (2007).